RESEARCH PAPER

Synthesis and characteristics of CMK-3 modified with magnetite nanoparticles for application in hydrogen storage

Lisandro F. Venosta · Juliana M. Juárez · Oscar A. Anunziata · Paula G. Bercoff · Marcos B. Gómez Costa

Abstract In this work, we report the synthesis and characterization of iron oxide nanoparticles supported in nanostructured carbon (CMK-3). This material is promising in the application of hydrogen adsorption for energy storage. The material with iron oxide nanoparticles (Fe-CMK-3) was successfully synthesized and characterized by X-ray diffraction, textural properties analysis, transmission and scanning electron microscopy, X-ray photoelectron spectroscopy, and magnetization studies. A large amount of the iron incorporated as iron oxide nanoparticles was in the magnetite phase. The incorporation of magnetite on the CMK-3 carbon surface significantly improved the storage capacity of hydrogen (4.45 wt% at 77 K and 10 bar) compared with the CMK-3 framework alone (2.20 wt% at 77 K and 10 bar). The synthesized material is promising for hydrogen adsorption by weak bond forces (physisorption). A hydrogen adsorption mechanism was proposed in which the nanoparticles of magnetite have an important role.

L. F. Venosta · J. M. Juárez (✉) · O. A. Anunziata ·
M. B. Gómez Costa
Centro de Investigación en Nanociencia y Nanotecnología
(NANOTEC), Facultad Regional Córdoba, Universidad
Tecnológica Nacional, Maestro López y Cruz Roja,
5016 Córdoba, Argentina
e-mail: jjuarez@frc.utn.edu.ar

L. F. Venosta · P. G. Bercoff
Facultad de Matemática, Astronomía, Física y Computación
(FAMAF), Universidad Nacional de Córdoba, IFEG, CONICE,
Medina Allende s/n, Ciudad Universitaria, Córdoba, Argentina

Introduction

In the past decades, many researchers have paid special attention to hydrogen storage, because it is an effective, cheap, and clean energy carrier with a nominal capacity of 243 kJ/mol. It can be used not only for fuel cell vehicles but also in portable devices. The main advantage of hydrogen as a perfect substitute to fossil resources is that it tackles both energy and environmental problems at the same time (Froudakis 2011; Dutta 2014; Satyapal et al. 2007; Armoli and Balzani 2011; Liu et al. 2010).

Even though hydrogen has a high heating value per unit mass, it is renewing, it is eco-friendly, and it has a kinetics for adsorption-desorption that can be considered simple, a viable H_2 storage system is critical. Among the disadvantages, storage and transport problems must be solved (Langmi et al. 2014). Therefore, the current scientific challenge is to design a lightweight, low-cost nanostructured material that can be used as a "hydrogen sponge," with a reversible hydrogen uptake at room temperature (Wang et al. 2010).

Different materials such as zeolites, activated carbons, and MOFs have been widely studied in this field of application (Liu et al. 2007; Li and Yang 2006; Park et al. 2008; Kim et al. 2008; Dong et al. 2007). The hydrogen storage capacity of these materials is related to the van der Waals interactions between the surface of

the materials and hydrogen molecules (Hirscher et al. 2010). Therefore, materials with large surface areas and low densities, such as nanostructured mesoporous carbons, have been studied for this purpose. In recent years, different synthesis methods have been developed to obtain mesoporous carbon materials with various textural properties (Jun et al. 2000; Lu et al. 2005).

Mesostructured carbons from Korea (CMK) belong to a family of ordered mesoporous carbons (OMC) (Yang and Zhao 2005). This kind of materials can be synthesized by a nanocasting strategy inside the channels of mesostructured aluminosilicates, used as true "nanoreactors." The carbons are obtained through this method using an inorganic template agent, by the introduction of suitable carbon precursors into the ordered pores of the mesoporous material based on silicates (SBA-15), followed by carbonization and finally the elimination of the precursors. They have specific surfaces from 1000 to 2000 m^2/g and pore volumes from 0.5 to 1 mL/g (Jun et al. 2000; Joo et al. 2001). This highly ordered carbon material (CMK-3) with a large surface area, high chemical stability, uniform pore diameter, accessible porosity, and three-dimensional channel network is a good candidate for use in hydrogen storage (Anbia and Ghaffari 2009; Anbia and Parvin 2011).

The incorporation of metal or metal oxide nanoparticles promotes the presence of active sites, which has been recognized as a viable way to improve hydrogen storage capacity (Giasafaki et al. 2012). The nanoparticles dispersed within the pores of the nanostructured carbons contribute greatly to improve the hydrogen storage capacities. In the case of materials with noble metals incorporated into the structure, atomic hydrogen diffuses more deeply into the microporous network of the carbon and even between the graphitic layers reaching the metallic particle, where the adsorption would take place by means of a spillover effect. Although it was demonstrated that metals like platinum or palladium improve the behavior of this mechanism, other studies present better results using more cost-effective metals (Giraudet and Zhu 2011). Clearly, the hydrogen adsorption capacity of carbon materials can be improved with the introduction of appropriate nanoparticles. Although it was found that the storage of hydrogen was rather proportional to the specific surface area, the micropore diameter can play a key role in the determination of the final storage capacity (Kim and Park 2011). In previous reports, we have proven that the

incorporation of different metal or metal oxide nanoparticles improves the hydrogen storage capability of mesoporous carbon. For instance Pt, Ni, Zn, TiO_2, and V_2O_5 nanoparticles, among others, incorporated into nanostructured carbon CMK-3 show larger hydrogen uptake at lower and higher pressures than CMK-3 (Juárez et al. 2015a; Juárez et al. 2015b; Juárez et al. 2017; Gómez Costa et al. 2013).

In this framework, the aim of the present paper is to study the hydrogen storage capacity of a mesoporous carbon CMK-3 modified with nanoparticles of iron oxide (Fe-CMK-3). Different textural and chemical properties were analyzed and discussed concerning the improvement of hydrogen adsorption at 77 K for low and high pressures (up to 10 bar).

Experimental

Synthesis of ordered mesoporous carbon CMK-3

The synthesis of the ordered mesoporous carbon was performed by nanocasting strategy using silica mesoporous material SBA-15 as template and sucrose as carbon source (Juárez et al. 2015a).

The siliceous template was prepared according to a previously reported method (Juárez et al. 2015a). Briefly, 20 g of P123 (poly(ethylene glycol)-block-poly(propylene glycol)-block-poly(ethylene glycol), EO20PO70EO20, P123-Sigma-Aldrich) used as a surfactant was immersed in a HCl 1-M solution. After complete dissolution of the P123, 40 g of silica source TEOS (tetraethylorthosilicate, 98%, Sigma-Aldrich) was added dropwise and stirred at 50 °C for 24 h. The resulting mixture was kept at 80 °C for 72 h inside a polypropylene bottle. Afterwards, the material was filtered and washed until pH 7. In order to remove the surfactant, the recovered solid was immersed in an ethanol-water mixture and desorbed with N_2 flow (20 mL/min) at 470 °C for 4 h. Finally, a calcination procedure was performed at 550 °C for 4 h.

The SBA-15 synthesized was used as template for the synthesis of the mesoporous carbon. The previously described procedure (Juárez et al. 2015a) was as follows: Firstly, 1.1 g of sucrose was dissolved in an acid solution (5.0 g of deionized water and 0.14 g of H_2SO_4); the siliceous template was immersed in this solution, and heated afterwards for 6 h at 100 °C. After that time, the material was heated to 160 °C for another 6 h. A

second impregnation was carried out in order to ensure the infiltration of the sucrose within the pores of the siliceous template; the solutions involved in this impregnation process were the following: 0.65 g of sucrose, 90 mg of H_2SO_4, and 5.0 g of deionized water. Two thermal treatments at 100 °C and 160 °C for 6 h each were performed to the obtained material. The carbonization process was carried out at 900 °C for 4 h in inert atmosphere (N_2, 20 mL/min).

Finally, to remove the siliceous template, the composite was immersed in a solution of hydrofluoric acid (5 wt%) at room temperature. The resulting material was filtered, washed with an ethanol-water solution, and dried at 50 °C.

Synthesis of ordered mesoporous carbon with magnetite nanoparticles

The material modified with magnetite nanoparticles (Fe-CMK-3) was prepared by wet impregnation using $FeCl_3 \cdot 6H_2O$ as the iron source. This source was dissolved in deionized water and the CMK-3 support was incorporated to this solution. The mixture was placed in a rotary evaporator in order to remove the excess water at 60 °C and 60 rpm. Afterwards, the sample was dried at 100 °C overnight. Finally, the modified mesoporous carbon was then desorbed in an inert atmosphere (N_2, 20 mL/min) at 550 °C for 4 h. The theoretical percentage of incorporated iron was 2 wt%, in excellent agreement with ICP measurements (1.98%).

Characterization

Elemental analysis was performed by inductively coupled plasma-atomic emission spectroscopy (ICP) in a VISTA-MPX spectrometer, operated with a high-frequency emission power of 1.5 kW and plasma air flow of 12.0 L/min. The X-ray diffractogram was obtained with a Panalytical Philips X'pert XDS diffractometer with a Cu Kα radiation source. Nitrogen adsorption-desorption isotherms and pore size distribution were measured in a high-speed gas sorption analyzer (Nova 4000) after outgassing the samples at 200 °C for 4 h. N_2 adsorption-desorption isotherms and surface area measurements were carried out on a sorption equipment with an accuracy higher than 3% and a reproducibility of $\pm 0.5\%$. The pore size distribution (PSD) was estimated using the nonlocal density functional theory (NLDFT) algorithm from adsorption

isotherms. Prior to the measurement, the sample was outgassed for 12 h at 200 °C. TEM micrographs were taken in a TEM Philips EM 301 instrument. Direct current electrical conductivity measurements were performed using pellets, improving contact with a silver layer. Magnetic properties measurements of the samples were performed with a Lakeshore 7300 vibrating sample magnetometer (VSM). Hysteresis loops were measured by applying magnetic fields between ± 1.2 T, at room temperature. Scanning electron microscopy images were obtained with a FE-SEM, Sigma Zeiss equipment applying a voltage of 5 kV. XPS measurements were performed in a K-Alpha™ + X-ray photoelectron spectrometer (XPS) with an X-ray beam size of 400 μm. The spectrum was calibrated to the binding energy of the C–C carbon signal. Hydrogen storage isotherms at 77 K at low and high pressure (up to 10 bar) were measured using an ASAP 2050 equipment properly calibrated.

Results and discussion

X-ray diffraction

Low-angle X-ray diffractograms for CMK-3 and Fe-CMK-3 are shown in Fig. 1a. The CMK-3 nanostructured carbon, obtained with SBA-15 inorganic template, shows a structural order comparable with the P6mm, with a crystallographic hexagonal group, which is an exact replica of the SBA-15 (Yang and Zhao 2005).

The diffractogram of the iron-modified sample at low angle (Fig. 1a) is shifted to higher 2θ due to the oxide incorporation inside the channels of the mesoporous carbon that leads to a slight distortion in the structural regularity, and a little disorder and small shrinkage of the framework because of heating treatment and formation of more micropores during the activation process. Magnetite nanoparticles produce a minor alteration in the uniformity of channels that disturbs the distance of hexagonal regularity manifested with the shift observed at higher diffraction angles. This phenomenon was also observed before (Gómez Costa et al. 2013; Ding et al. 2015; Chaliha and Bhattacharyya 2009).

Figure 1b shows the high-angle X-ray diffractograms of the iron-modified material before (Fe-CMK-3) and after (Fe-CMK-3-H) hydrogen adsorption measurements. There are two wide peaks that correspond to the typical reflections (002) and (100) of graphitic
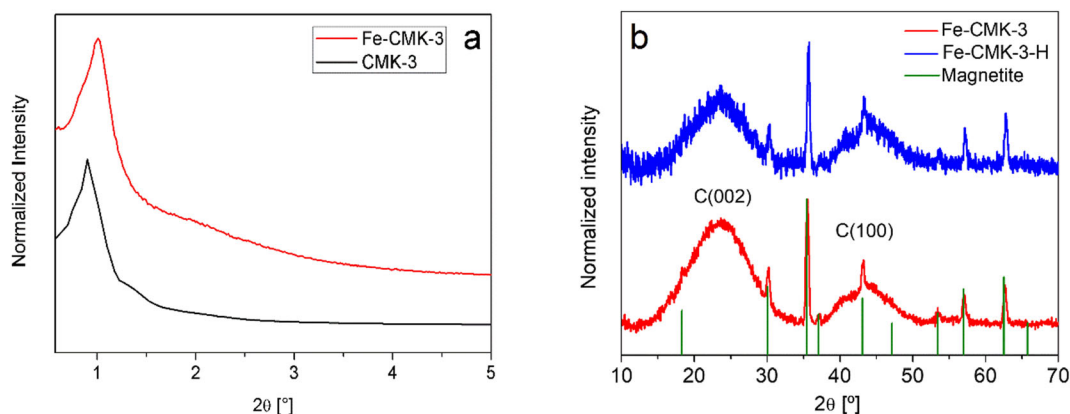
Fig. 1 X-ray diffractograms at: **a** low angle of CMK-3 and Fe-CMK-3 and **b** high angle of Fe-CMK-3 and Fe-CMK-3-H (sample modified with iron after hydrogen adsorption). The vertical lines correspond to the position of the spinel reflections

carbons (Suryavanshi et al. 2012). The characteristic reflections of the iron oxide corresponding to the spinel structure of magnetite (Fe_3O_4) are also observed: (220), (311), (400), (422), (511), and (440), located at approximately 30.3°, 35.7°, 43.3°, 53.7°, 57.2°, and 62.8°, respectively (PDF2 database: 00-019-0629). No other phases are observed, within the detection limits of this technique. This result indicates that the iron incorporated to the CMK-3 structure is in the form of magnetite nanoparticles with crystal size of approximately 18 nm for both samples, as estimated by the Scherrer equation.

It can be seen from the Fig. 1b that the presence of magnetite nanoparticles does not affect the carbon structure and that hydrogen storage does not modify the iron oxide nanoparticles.

Textural properties

CMK-3 and Fe-CMK-3 nitrogen adsorption/desorption isotherms (before and after hydrogen adsorption test) at 77 K are observed in Fig. 2, which shows a type IV H2 behavior with physisorption hysteresis, according to the typical IUPAC catalog of ordered nanoporous materials.

The materials synthesized exhibit capillary condensation, associated with a pore obstruction effect that affects the pressure where vaporization or desorption occurs. Figure 2b also shows the PSD of samples, showing narrow peaks indicating well-defined pores. The iron samples show a lower specific surface area and a smaller pore size (diameter) compared with CMK-3 (Table 1), which indicates that magnetite nanoparticles are within the mesoporous channels of the CMK-3 framework.

Scanning and transmission electron microscopy

Figure 3 shows SEM images of sample Fe-CMK-3.

The average size of the particles deposited on the surface of the CMK-3 support was obtained by a statistical analysis of several images giving $D \sim 40$ nm. This particle size is consistent with the crystal size estimated by the Scherrer equation from the measured diffractograms, indicating that the magnetite nanoparticles deposited on the surface of the carbonaceous framework are polycrystalline.

TEM images of the samples were obtained in order to study the structure and the size of the pores (Fig. 4).

The TEM image shows that nanometric particles are widely dispersed within the mesoporous structure of CMK-3. The average particle size was statistically calculated from several images, being $D \sim 4$ nm, as shown in the histogram of Fig. 4b.

Fe-CMK-3 contains a large number of smaller magnetite nanoparticles in the internal channels (of size around 4 nm), in addition to the larger particles detected by SEM ($D \sim 40$ nm) located at the external surface.

XPS

XPS results of sample Fe-CMK-3 are shown in Fig. 5 and the characteristic parameters are given in Table 2. In the case of CMK-3, the binding energy of C1s at approximately 284 eV is attributed to C–C sp3 and the peak at 286 eV is assigned to C=C sp2, both characteristic of CMK as graphite and disordered carbon species (Gardner et al. 1995; Darmstadt et al. 2003; Weidenthaler et al. 2006; Tang et al. 2010).
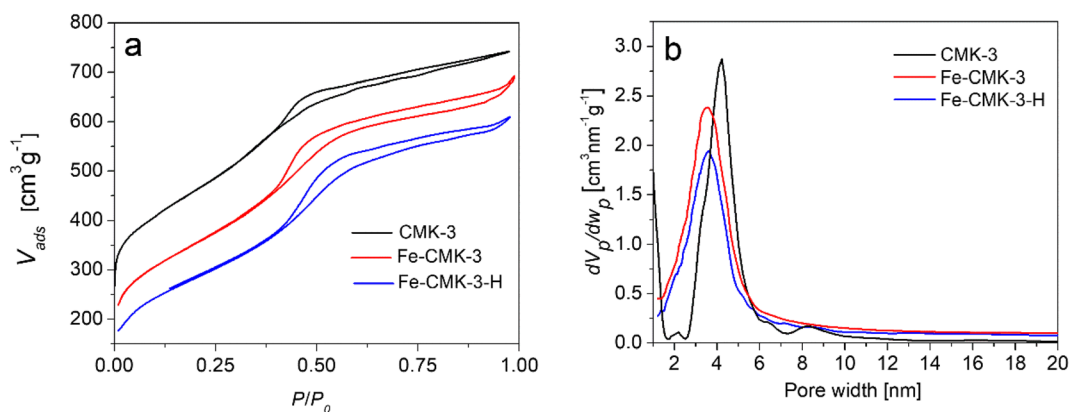
Fig. 2 **a** Nitrogen adsorption/desorption analysis (measured at standard temperature and pressure). **b** PSD of CMK-3 and Fe-CMK-3 before and after the hydrogen uptake test

Figure 5a shows the complete XPS spectrum of Fe-CMK-3, where the signals for iron, carbon, and oxygenated species can be identified. Figure 5b shows the peaks around 724.8 eV and 711.8 eV corresponding to the doublet of the $2p_{1/2}$ and $2p_{3/2}$ signals of magnetite (Fe_3O_4). It has been previously reported that the peak positions for pure Fe_3O_4 of Fe $2p_{1/2}$ and Fe $2p_{3/2}$ are, respectively, 724.1 eV and 711.4 eV (Tan et al. 1990; Allen et al. 1974; Hawn and DeKoven 1987; Muhler et al. 1992; Yamashita and Hayes 2008). Despite the low resolution of the measurement in this energy range (due to the low Fe content in the sample), it can be stated that metallic iron is not present, within the limit of detection of this technique. In general, the line associated with this metal should appear as a shoulder of the peak $2p_{3/2}$, at 706.7 eV. Figure 5c shows the characteristic bands of oxygen, the C–O band and the corresponding to O linked with metal cations (magnetite). There is also an unidentified band associated with organic molecules, which could be attributed to sucrose that has not been fully carbonized in the synthesis process (Nordfors et al. 1991). In Fig. 5d, C–

C and C=C bonds can be observed, mainly due to the carbon matrix of the CMK-3 and traces of C–O and C=O bonds, because of the possible existence of some oxygenated compounds on the surface of CMK-3. Finally, traces of organic compounds appear that are remnants of the synthesis process of this carbon. The other fitted bands correspond to satellite lines of the main magnetite features, and FeO traces with their respective satellite bands.

The XPS analysis agrees with the results of high-angle XRD and confirms that the impregnated iron has oxidized to magnetite. The low amount of iron oxide on the surface suggests that iron species are mainly found in the inner channels of the mesoporous carbon. The Fe 2p wt% of approximately 1.4% (see Table 2) indicates that iron is well distributed both on the surface and inside the CMK-3 channels. According to ICP results for iron content (1.98 wt%), it is possible to deduce that there is a larger amount of smaller magnetite nanoparticles inside the channels than outside, where bigger nanoparticles are found. The Fe/C atomic ratio is 0.003 which would indicate that the magnetite is highly dispersed within the carbonaceous material.

Table 1 Textural properties of CMK-3 and Fe-CMK-3 before and after H adsorption

Sample	Surface area (m^2/g)	Pore volume (cm^3/g)	Pore size (nm)
CMK-3	1323	1.01	4.2
Fe-CMK-3	1237	0.98	3.6
Fe-CMK-3-H	1231	0.97	3.6

Pore diameter: calculated by the NLDFT method (Ravikovitch et al. 1998)
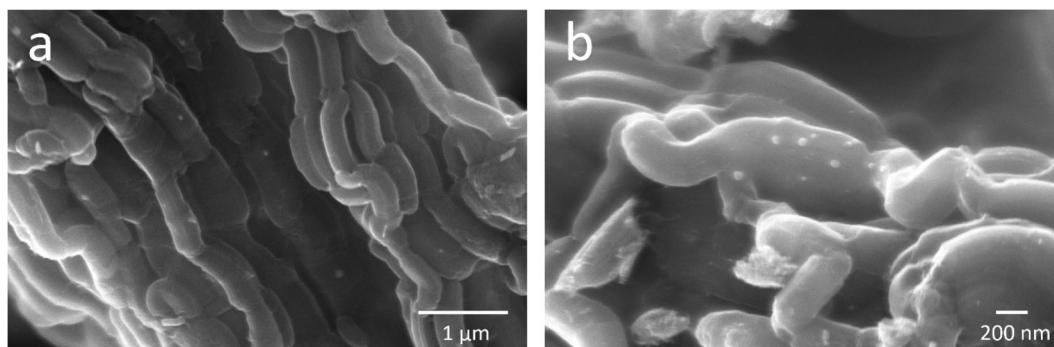
Fig. 3 SEM images of iron-modified CMK-3 (Fe-CMK-3) taken at different magnifications. Magnetite nanoparticles are observed as bright spots on the surface of the carbonaceous support

Magnetic properties

The magnetization M versus applied magnetic field H hysteresis loop of sample Fe-CMK-3 is shown in Fig. 6, after subtracting the diamagnetic contribution of the carbon.

The curve corresponds to a ferromagnetic signal in agreement with the presence of magnetite, displaying a coercive field of 20 mT and a saturation magnetization of 1.4 emu/g of the composite (this corresponds to ~ 70 emu/g of magnetite, since the estimated weight fraction of magnetite present in the sample is ~ 2 wt%). These values agree with those for magnetite nanoparticles of ~ 40 nm (Batlle et al. 2011) and correspond to the particles located at the surface of the carbonaceous structures, as determined by SEM (see Fig. 3). The particles inside the channels of size $D \sim 4$ nm (as determined by TEM, Fig. 4) are superparamagnetic (Upadhyay et al. 2016) and have negligible coercivity but contribute to the total magnetization.

Hydrogen adsorption measurements

With the purpose of evaluating the hydrogen uptake capacity (Juárez et al. 2015b), hydrogen adsorption/desorption measurements at 77 K were performed on samples CMK-3 and Fe-CMK-3 in a pressure range 0–10 bar. The obtained curves can be observed in Fig. 7.

Experimental information were fit with the Freundlich isotherm equation, which is an empirical expression used in gas adsorption studies. To fit the experimental data, a nonlinear regression of least squares was used, and an optimization numerical method (Levenberg-Marquardt) was employed. The fitting regression coefficient was 0.98, indicating good accuracy.

In the whole pressure range, the amount of adsorbed hydrogen is larger in the iron-containing sample. The process is completely reversible as it can be seen in Fig. 7, by the superposition of the absorption and desorption data points. The presence of magnetite nanoparticles
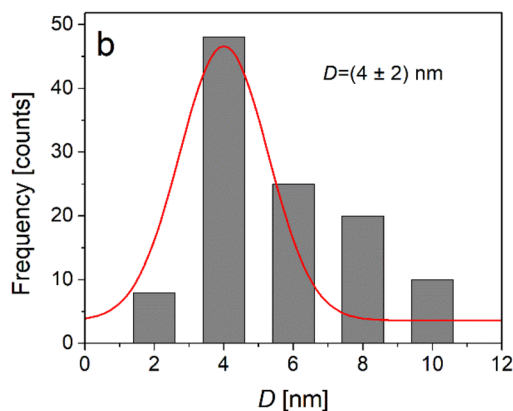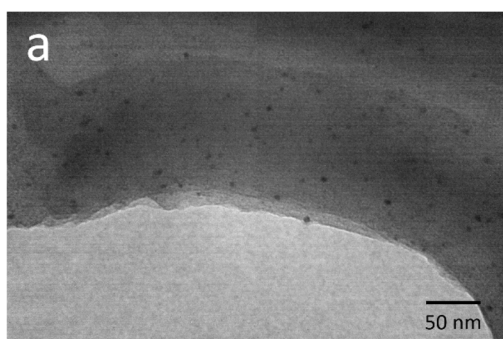
Fig. 4 **a** Fe-CMK-3 TEM image and **b** particle size distribution analysis
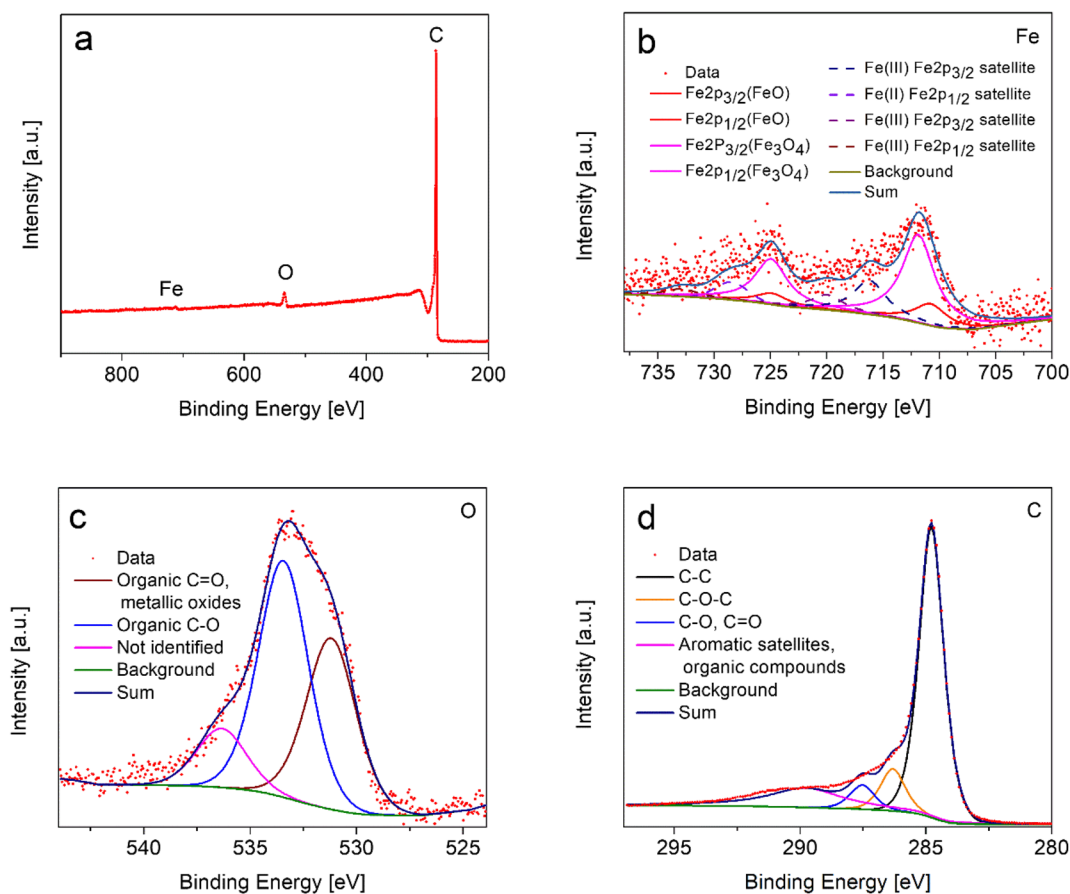
Fig. 5 **a** High-resolution XPS spectrum of Fe-CMK-3 and regions corresponding to signals of **b** iron, **c** oxygen, and **d** carbon

increases the hydrogen adsorption capacity of the CMK-3 alone. Magnetite aggregates are better dispersed helped by the CMK-3 surface; therefore, the nanoparticles are smaller and the activity for hydrogen storage increases due to a larger surface area of magnetite nanoparticles and its high dispersion.

Table 2 Binding energy (BE), at.% and wt% of C, O, and Fe in Fe-CMK-3

	BE (eV)	at.%	wt%
C1s	284.78	96.06	93.88
	286.28		
	287.48		
	289.88		
O1s	531.18	3.63	4.73
	533.48		
	536.33		
Fe 2p	711.93	0.31	1.39
	725.03		

There are two important mechanisms of charge transfer in hydrogen adsorption. On the one hand, the hydrogen molecule is a weak Lewis acid donating charges from its σ orbital. In contrast, it functions as a weak base
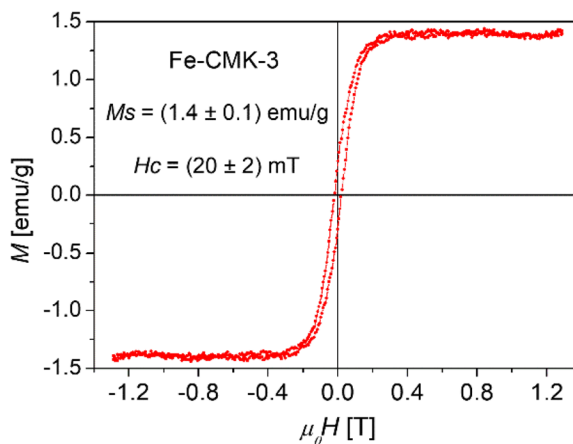
Fig. 6 Magnetization hysteresis loop of Fe-CMK-3 after subtracting the diamagnetic background (Venosta et al. 2017)
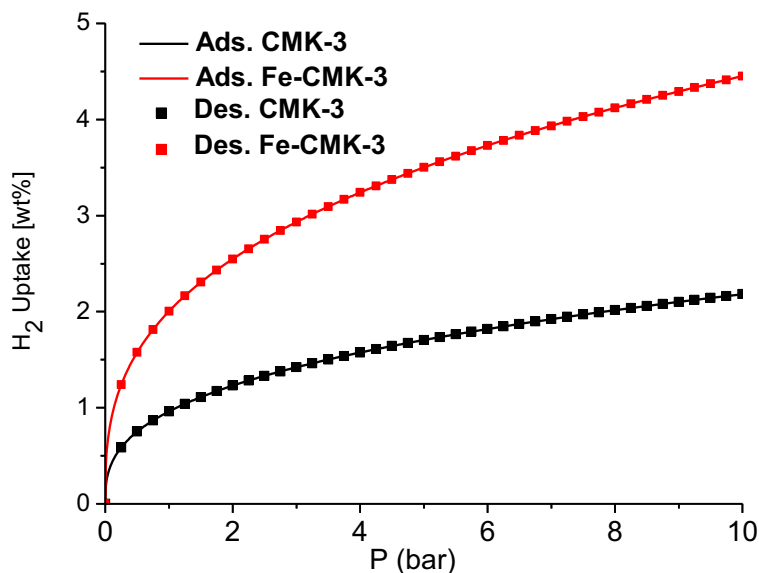
Fig. 7 Hydrogen adsorption (solid lines)/desorption (squares) curves of CMK-3 and Fe-CMK-3 at 77 K

of Lewis where the σ* orbital of the hydrogen molecule accepts the charge of the adsorbent. An important contribution to H_2 physisorption can be found within the phenomenon of polarization, creating electrostatic moments in the H_2 molecule. This allows an attractive electrostatic interaction with the linker. A polarization of the hydrogen molecule could cause a strong dipole or quadrupole moment.

Studies (Hoang and Antonelli 2009) show that the surface area is not the only important factor in hydrogen storage and that hydrogen bonding increases with the oxidation state, provided that this factor is not compensated by other parameters. It also demonstrates that an enthalpy increase in surface coverage occurs whenever there is a transition metal with d electrons on the surface.

The reason for this increase is not yet understood, but calculations by Yildirim and Ciraci (Yildirim and Ciraci 2005) predict an increase in binding enthalpy with increasing hydrogen ligation in Kubas compounds with multiple H_2 ligands.

In this study, CMK-3 carbon acts as a framework to support magnetite nanoparticles for Kubas binding to hydrogen.

According to studies (Yildirim and Ciraci 2005) in nanotubes decorated with Ti, the first hydrogen molecule dissociates into two hydrides by oxidative addition to magnetite. During this process, the H–H distance increases. The second, third, and fourth hydrogen

molecules bind to the magnetite nanoparticle without dissociation in Kubas type interaction. Yildirim's calculations show that the system is stable until four hydrogen molecules are adsorbed.

Therefore, this adsorption mechanism is similar to that described in this work for the magnetite-decorated CMK-3 in that it uses a carbon support as a graft site for Kubas binding of hydrogen.

Assuming that weak orbital interactions occur between H_2 and magnetite active site, it is possible to say that the first coat of hydrogen molecules can react with dissociation on magnetite nanoparticle. Second, third, and fourth layers interact with magnetite of Fe-CMK-3 through a metal-dihydrogen complex (Kubas complex) (Takasu et al. 1978). More layers could link with the metal oxide particles by induced dipole forces because

Table 3 Hydrogen adsorption of different nanomaterials

Material	Hydrogen uptake (wt%)*	Reference
Pt-CMK-3	3.3	(Juárez et al. 2015a)
Anatase-CMK-3	2.9	(Gómez Costa et al. 2017)
Ti-CMK-3	2.6	(Juárez et al. 2017)
VxOy-CMK-3	3.43	(Juárez et al. 2019)

*H_2 sorption at 10 bars and 77 K

the strong interaction between magnetite nanoparticles and hydrogen molecules induces dipole forces and it is possible that more H_2 molecules are adsorbed in more coats by dipole-dipole-like interactions, but the link forces diminish when the distance to Fe-CMK-3 surface increases.

In previous works, we have studied the effect on hydrogen adsorption of different mesoporous carbons modified with different nanoparticles (Table 3). The hydrogen adsorption capacity depends not only on the surface area of the nanomaterial but also on the size and characteristics of the nanoparticles that modify it.

Conclusion

A significant result of this research related to hydrogen adsorption and storage refers to the design of ordered mesoporous carbon modified with magnetite nanoparticles. This material adsorbs hydrogen molecules through weak bond forces (physisorption). The activity of the samples is due to a high surface area of both the mesoporous carbon and the exposed surface of the magnetite nanoparticles as well as the uniform dispersion of this.

In this work, a mechanism is proposed explaining how hydrogen molecules are adsorbed on the sample and the difference in adsorption between the Fe-CMK-3 material and the support.

We are in the process of optimization and improvement of the material to increase the adsorption of hydrogen and therefore increase the storage capacity. This optimization in adsorption capacity can be done through the control of the size and dispersion of the nanoparticles and the type of support.

Compliance with ethical standards

Conflict of interest The authors declare that they have no conflict of interest.

References

Allen GC, Curtis MT, Hooper AJ, Tucker PM (1974) X-ray photoelectron spectroscopy of iron–oxygen systems. J Chem Soc Dalton Trans 14:1525–1530. https://doi.org/10.1039/DT9740001525

Anbia M, Ghaffari A (2009) Adsorption of phenolic compounds from aqueous solutions using carbon nanoporous adsorbent coated with polymer. Appl Surf Sci 255:9487–9492. https://doi.org/10.1016/j.apsusc.2009.07.070

Anbia M, Parvin Z (2011) Desulfurization of fuels by means of a nanoporous carbon adsorbent. Chem Eng Res Des 89:641–647. https://doi.org/10.1016/j.cherd.2010.09.014

Armoli N, Balzani V (2011) The hydrogen issue. Chem Sus Chem 4:21–36. https://doi.org/10.1002/cssc.201000182

Batlle X, Pérez N, Guardia P, Iglesias O, Labarta A, Bartolomé F, Serna CJ (2011) Magnetic nanoparticles with bulklike properties. J Appl Phys 109:07B524. https://doi.org/10.1063/1.3559504

Chaliha S, Bhattacharyya KG (2009) Fe(III)-, Co(II)- and Ni(II)-impregnated MCM41 for wet oxidative destruction of 2,4-dichlorophenol in water. Catal Today 141:225–233. https://doi.org/10.1016/j.cattod.2008.03.011

Darmstadt H, Roy C, Kaliaguine S, Kim TW, Ryoo R (2003) Surface and pore structures of CMK-5 ordered mesoporous carbons by adsorption and surface spectroscopy. Chem Mater 15:3300–3307. https://doi.org/10.1021/cm020673b

Ding W, Zhu W, Xiong J, Yang L, Wei A, Zhang M, Li H (2015) Novel heterogeneous iron-based redox ionic liquid supported on SBA-15 for deep oxidative desulfurization of fuels. Chem Eng J 266:213–221. https://doi.org/10.1016/j.cej.2014.12.040

Dong J, Wang X, Xu H, Zhao Q, Li J, Dong J, Wang X, Xu H, Zhao Q, Li J (2007) Hydrogen storage in several microporous zeolites. Int J Hydrog Energy 32:4998–5004. https://doi.org/10.1016/j.ijhydene.2007.08.009

Dutta S (2014) A review on production, storage of hydrogen and its utilization as an energy resource. J Ind Eng Chem 20:1148–1156. https://doi.org/10.1016/j.jiec.2013.07.037

Froudakis GE (2011) Hydrogen storage in nanotubes & nanostructures. Mater Today 14:324–328. https://doi.org/10.1016/S1369-7021(11)70162-6

Gardner SD, Singamsetty CSK, Booth GL, He G (1995) Surface characterization of carbon fibers using angle-resolved XPS and ISS. Carbon 33:587–595. https://doi.org/10.1016/0008-6223(94)00144-O

Giasafaki D, Bourlinos A, Charalambopoulou G, Stubos A, Steriotis TH (2012) Synthesis and characterisation of nanoporous carbon–metal composites for hydrogen storage. Microporous Mesoporous Mater 154:74–81. https://doi.org/10.1016/j.micromeso.2011.11.011

Giraudet S, Zhu Z (2011) Hydrogen adsorption in nitrogen enriched ordered mesoporous carbons doped with nickel nanoparticles. Carbon 49:398–405. https://doi.org/10.1016/j.carbon.2010.09.035

Gómez Costa MB, Juárez JM, Martínez ML, Beltramone AR, Cussa J, Anunziata OA (2013) Synthesis and characterization

of conducting polypyrrole/SBA-3 and polypyrrole/Na–AlSBA-3 composites. Mat Res Bull 48:661–667. https://doi.org/10.1016/j.materresbull.2012.11.030

Gómez Costa MB, Juárez JM, Pecchi G, Anunziata OA (2017) Anatase–CMK-3 nanocomposite development for hydrogen uptake and storage. Bull Mater Sci 40:271–280. https://doi.org/10.1007/s12034-017-1382-4

Hawn DD, DeKoven BM (1987) Deconvolution as a correction for photoelectron inelastic energy losses in the core level XPS spectra of iron oxides. Surf Interface Anal 10:63–74. https://doi.org/10.1002/sia.740100203

Hirscher M, Panella B, Schmitz B (2010) Metal-organic frameworks for hydrogen storage. Micropor Mesopor Mater 129:335–339. https://doi.org/10.1016/j.micromeso.2009.06.005

Hoang TKA, Antonelli DM (2009) Exploiting the Kubas interaction in the design of hydrogen storage materials. Adv Mater 21:1787–1800. https://doi.org/10.1002/adma.200802832

Joo SH, Jun S, Ryoo R (2001) Synthesis of ordered mesoporous carbon molecular sieves CMK-1. Microporous Mesoporous Mater 44:153–158. https://doi.org/10.1016/S1387-1811(01)00179-2

Juárez JM, Gómez Costa MB, Anunziata OA (2015a) Synthesis and characterization of Pt-CMK-3 hybrid nanocomposite for hydrogen storage. Int J Energy Res 39:128–139. https://doi.org/10.1002/er.3229

Juárez JM, Gómez MB, Anunziata OA, (2015b) Preparation and characterization of activated CMK-1 with Zn and Ni species applied in hydrogen storage. Int J Energy Res 39:941- Juárez JM 953. https://doi.org/10.1002/er.3298

Juárez JM, Ledesma BC, Gómez Costa MB, Beltramone AR, Anunziata OA (2017) Novel preparation of CMK-3 nanostructured material modified with titania applied in hydrogen uptake and storage. Microporous and Mesoporous Mater 254:146–152. https://doi.org/10.1016/j.micromeso.2017.03.056

Juárez JM, Gómez Costa MB, Martínez ML, Anunziata OA (2019) Influence of vanadium nanoclusters in hydrogen uptake using hybrid nanostructured materials. J Porous Mater 26:951–959. https://doi.org/10.1007/s10934-018-0689-x

Jun S, Hoo JS, Ryoo R, Kruk M, Jaroniec M, Liu Z, Ohsuna T, Terasaki O (2000) Synthesis of new, nanoporous carbon with hexagonally ordered mesostructure. J Am Chem Soc 122:10712–10713. https://doi.org/10.1021/ja002261e

Kim BJ, Park SJ (2011) Optimization of the pore structure of nickel/graphite hybrid materials for hydrogen storage. Int J Hydrogen Ener 36:648–653. https://doi.org/10.1016/j.ijhydene.2010.09.097

Kim BJ, Lee YS, Park SJ (2008) Preparation of platinum-decorated porous graphite nanofibers, and their hydrogen storage behaviors. Colloid Interface Sci 318:530–533. https://doi.org/10.1016/j.jcis.2007.10.018

Langmi HW, Ren J, North B, Mathe M, Bessarabov D (2014) Hydrogen storage in metal-organic frameworks: a review. Electrochim Acta 128:368–392. https://doi.org/10.1016/j.electacta.2013.10.190

Li Y, Yang RT (2006) Hydrogen storage in metal−organic frameworks by bridged hydrogen spillover. J Am Chem Soc 128:8136–8137. https://doi.org/10.1021/ja061681m

Liu YY, Zeng JL, Zhang J, Xu F, Sun LX (2007) Improved hydrogen storage in the modified metal-organic frameworks by hydrogen spillover effect. Int J Hydrog Energy 32:4005–4010. https://doi.org/10.1016/j.ijhydene.2007.04.029

Liu C, Li F, Ma LP, Chen HM (2010) Advanced materials for energy storage. Adv Mater 22:28–62. https://doi.org/10.1002/adma.200903328

Lu A, Li WC, Schmidt W, Schüth F (2005) Template synthesis of large pore ordered mesoporous carbon. Microporous Mesoporous Mater 80:117–128. https://doi.org/10.1016/j.micromeso.2004.12.007

Muhler M, Schlögl R, Ertl G (1992) The nature of the iron oxide-based catalyst for dehydrogenation of ethylbenzene to styrene 2. Surface chemistry of the active phase. J Catal 138:413–444. https://doi.org/10.1016/0021-9517(92)90295-S

Nordfors D, Nilsson A, Martensson N, Svensson S, Gelius U (1991) X-ray excited photoelectron spectra of free molecules containing oxygen. J Electron Spectrosc 56:117–164. https://doi.org/10.1016/0368-2048(91)80009-J

Park SJ, Kim BJ, Lee YS, Cho MJ, Park SJ, Kim BJ, Lee YS, Cho MJ (2008) Influence of copper electroplating on high pressure hydrogen-storage behaviors of activated carbon fibers. Int J Hydrog Energy 33:1706–1710. https://doi.org/10.1016/j.ijhydene.2008.01.011

Ravikovitch PI, Haller GL, Neimark AV (1998) Pore size analysis of MCM-41 type adsorbents by means of nitrogen and argon adsorption. J Colloid Interface Sci 207:159–169. https://doi.org/10.1006/jcis.1998.5748

Satyapal S, Petrovic J, Read C, Thomas G, Ordaz G (2007) The U.S. Department of Energy's National Hydrogen Storage Project: progress towards meeting hydrogen-powered vehicle requirements. Catal Today 120:246–256. https://doi.org/10.1016/j.cattod.2006.09.022

Suryavanshi U, Iijima T, Hayashia A, Hayashi Y, Tanemura M (2012) Fabrication of ZnO nanoparticles confined in the channels of mesoporous carbon. Chem Eng J 179:388–393. https://doi.org/10.1016/j.cej.2011.10.087

Takasu Y, Unwin R, Tesche B, Bradshaw AM, Grunze M (1978) Photoemission from palladium particle arrays on an amorphous silica substrate. Surf Sci 77:219–232. https://doi.org/10.1016/0039-6028(78)90003-1

Tan BJ, Klabunde KJ, Sherwood PM (1990) Studies of Pt-Sn/Al2O3 catalysts prepared by Pt and Sn coevaporation (solvated metal atom dispersion). J Catal 126:173–186. https://doi.org/10.1016/0021-9517(90)90055-O

Tang Z, He X, Song Y, Liu L, Guo Q, Yang J (2010) Properties of mesoporous carbons prepared from different carbon precursors using nanosize silica as a template. New Carbon Mater 25:465–469. https://doi.org/10.1016/S1872-5805(09)60045-7

Upadhyay S, Parekh K, Pandey B (2016) Influence of crystallite size on the magnetic properties of Fe3O4 nanoparticles. J Alloys Compd 678:478–485. https://doi.org/10.1016/j.jallcom.2016.03.279

Venosta L, Bracamonte MV, Rodríguez MC, Jacobo SE, Bercoff PG (2017) Comparative studies of hybrid functional materials based on different carbon structures decorated with nano-magnetite. Suitable application as platforms for enzyme-free electrochemical sensing of hydrogen peroxide. Sens Actuators B Chem 248:460–469. https://doi.org/10.1016/j.snb.2017.03.159

Wang CY, Tsao CS, Yu MS, Liao PY, Chung TY, Wu HC, Miller MA, Tzeng YR (2010) Hydrogen storage measurement, synthesis and characterization of metal–organic frameworks via bridged spillover. J Alloys Compd 492:88–94. https://doi.org/10.1016/j.jallcom.2009.11.203

Weidenthaler C, Lu AH, Schmidt W, Schüth F (2006) X-ray photoelectron spectroscopic studies of PAN-based ordered mesoporous carbons (OMC). Micropor Mesopor Mater 88: 238–243. https://doi.org/10.1016/j.micromeso.2005.09.015

Yamashita T, Hayes P (2008) Analysis of XPS spectra of Fe2+ and Fe3+ ions in oxide materials. Appl Surf Sci 254:2441–2449. https://doi.org/10.1016/j.apsusc.2007.09.063

Yang H, Zhao D (2005) Synthesis of replica mesostructures by the nanocasting strategy. Mater Chem 15:1217–1231. https://doi.org/10.1039/B414402C

Yildirim T, Ciraci S (2005) Titanium-decorated carbon nanotubes as a potential high-capacity hydrogen storage medium. Phys Rev Lett 94:175501–117550. https://doi.org/10.1103/PhysRevLett.94.175501

Publisher's note Springer Nature remains neutral with regard to jurisdictional claims in published maps and institutional affiliations.